Chemical Physics Letters 579 (2013) 51–57

Contents lists available at SciVerse ScienceDirect

Chemical Physics Letters

journal homepage: www.elsevier.com/locate/cplett

Vibrational and electronic relaxation in MEH-PPV using few cycle pulses

Takayoshi Kobayashi [a,b,c,d,*], Munenori Yamashita [a], Juan Du [a,b,*], Jun Zhang [a], Izumi Iwakura [a]

[a] Advanced Ultrafast Laser Research Center, University of Electro-Communications, Tokyo 182-8585, Japan
[b] CREST, Japan Science and Technology Agency, Tokyo 102-0076, Japan
[c] Department of Electrophysics, National Chiao Tung University, 3005, Taiwan
[d] Institute of Laser Engineering, Osaka University, Osaka 565-0971, Japan

ARTICLE INFO

Article history:
Received 16 April 2013
In final form 13 June 2013
Available online 24 June 2013

ABSTRACT

The electronic population decay time is determined to be about 500 fs in (poly-[2-methoxy-5-(2′-ethyl-hexyloxy)-*p*-phenylenevinylene] (MEH-PPV) using 5.7 fs pulses. The ultrafast electronic dephasing time and the self-trapping time of free exciton to form an exciton polaron is determined as 25 ± 2 fs and 50 ± 23 fs, respectively. Real-time spectrogram analysis reveals dynamic mode coupling among the high-frequency and low-frequency modes. The energy-ladder descent vibrational process is clarified using the first moment of the difference absorption spectrum. The phase relaxation time is calculated from the widths of the Fourier spectra of several strongly coupled modes.

1. Introduction

Conjugated polymers have been extensively studied because of their usefulness for various electro-optical (EO) and optoelectronic (OE) applications [1–12] and chemical modification [1–4,13–18]. Extensive study of poly-[2-methoxy-5-(2′-ethyl-hexyloxy)-*p*-phenylenevinylene] (MEH-PPV) has revealed that its luminescence process involves excitons [19–23]. The best method for clarifying the radiationless relaxation mechanism important for luminescence efficiency is transient spectroscopy [24–35]. The relaxation induces time-resolved spectral and intensity changes in the induced absorption and stimulated gain, which both originate from the imaginary part of the third-order nonlinear susceptibility. In contrast, the real part of the third-order susceptibility induces a phase change. Structural changes due to geometrical relaxation can be studied by the time dependent instantaneous vibrational frequencies of a photoexcited molecule. It is thus critical to clarify the vibronic coupling mechanism in radiationless relaxation mechanisms which determines the luminescence efficiency.

This Letter is organized as follows. Section 3.1 discusses ultrafast geometrical relaxation through self-trapping. Section 3.2 discusses the thermalization and electronic population relaxation. In Section 3.3, mechanism of observed modulation of difference transmission of the probe light is discussed. In Section 3.4, dynamic mode coupling among coherent vibrations is discussed using the spectrogram. Descent of the vibrational energy ladder is clarified which identifies the contributions of the modes to the thermalization process and the vibrational dephasing time is determined for several modes in Section 3.5. In Section 3.6, the electronic dephasing time is determined from data in the negative-time range.

2. Experimental

A noncollinear optical parametric amplifier (NOPA) [36,37] was used in the pump–probe experiment [27–29]. Briefly the pulse duration was 5.7 fs and the spectral range was 520–750 nm. The pump and probe pulses had energies of about 35 and 5 nJ, respectively. Chloroform solution of MEH-PPV was spin-coated on quartz plates. All experiments were performed at 293 ± 1 K.

3. Results and discussion

3.1. Ultrafast geometrical relaxation due to self-trapping

Figure 1 shows the laser spectrum and the absorption and fluorescence spectra, stimulated emission spectrum calculated based on spontaneous emission, and time-resolved spectra of the sample. Since the time-resolved spectrum was measured at 1-fs step and the spectral shapes at two succeeding delay times are clearly different from each other beyond the experimental error, it can be claimed that the spectrum has 1-fs time resolution. As shown in Figure 1, the time-resolved spectra were obtained by integration of spectra measured with the 1-fs resolution over a 100-fs probe delay time window centered at sixteen delay times ranging from 200 to 1700 fs in 100 fs steps. Integration over 100 fs is sufficient to remove spectral shifts and intensity changes induced by molecular vibrations with shorter periods than 20 fs. In one-dimensional systems such as MEH-PPV, after photoexcitation of a free exciton (FE), geometrical relaxation occurs to form a self-trapped exciton

* Corresponding authors at: Advanced Ultrafast Laser Research Center, University of Electro-Communications, Tokyo 182-8585, Japan. Fax: +81 42 443 5825.
E-mail addresses: kobayashi@ils.uec.ac.jp (T. Kobayashi), dujuan@mail.siom.ac.cn (J. Du).

0009-2614/$ - see front matter © 2013 Elsevier B.V. All rights reserved.
http://dx.doi.org/10.1016/j.cplett.2013.06.029

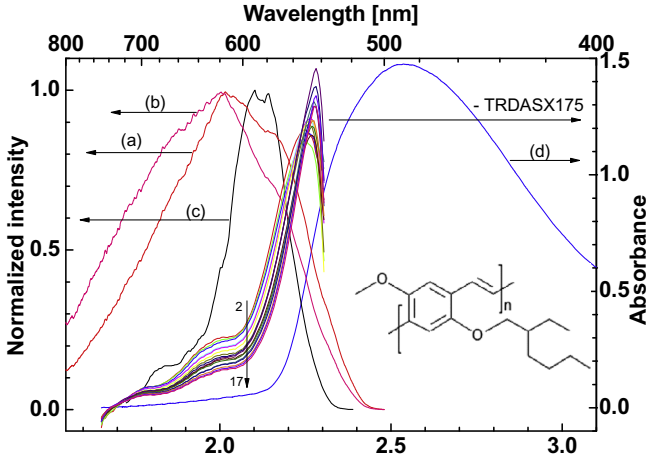

Figure 1. The spectra of spontaneous fluorescence (a), stimulated emission (b), pump laser (c), and absorption (d), and time-resolved difference absorption spectrum (TRDAS). Lines depicted with (e) from 2 to 17 are sixteen TRDAS calculated from 200 to 1700 fs with a 100-fs step. The corresponding units for the TRDAS are multiplied with (−175). The inset is the molecular structure of the MEH-PPV.

(STE). The time constants for geometrical relaxation in polydiacetylene (PDA) using a 4.7-fs pulse were determined as 62 ± 5 and 80 ± 5 fs at probe photon energies of 1.96 and 1.75 eV, respectively [28]. However, the time constant for geometrical relaxation in MEH-PPV could not be resolved due to the limited resolution due to the used pulse duration of 25 fs; it was determined as <120 fs [38].

Figure 2a shows traces of absorbance changes in 556–654 nm (2.23–1.90 eV). The absorbance change in the range 2.05–2.19 eV was fitted using the following equation involving two exponentials.

$$\Delta A = A\ \exp(-t/\tau_1) + B\ \exp(-t/\tau_2) + C \quad (1)$$

Outside of this region, the absorbance change could not be well fitted due to the coherent artifacts and the contribution of components which lasts longer >3 ps. For 605–565 nm (2.05–2.19 eV) the decay constants were calculated to be $\tau_1 = 50 \pm 23$ fs and $\tau_2 = 1.8 \pm 0.4$ ps. The large standard deviations is because of the simultaneous spectral shift and population decay as seen in Figure 1, and in the expanded spectra (Figure 3a and b). The constants τ_1 and τ_2 correspond to self-trapping and thermalization processes, respectively, based on similar relaxation processes in PDA [28]. Both are shorter for MEH-PPV than for PDA. The difference between the shorter time constant τ_1, associated with self-trapping, for the two polymers is discussed in the following.

The previously studied conjugated polymer, poly[5,7,17,19-tetracosatetraynylenebis(*N*-butoxycarbonylmethyl)carbamate] (PDA-4BCMU4A(8)), is a ladder polymer composed of two chains separated by methylene chains [39]. Consequently, this system has a dimensionality of two, so that excitons are not confined to a single dimension, and the one-dimensional barrierless potential model [28] is not exactly valid for it. In contrast, excitons in MEH-PPV are confined to a single dimension. Here, the polymer is considered to be one dimensional because the exciton size perpendicular to the main chain is smaller than the extension of the delocalized π electrons, which is considered to have four repeat-unit size [40], and is much larger than the extension of π-electron conjugation perpendicular to the main chain. Then there is no barrier between the FE and STE potential curves [28]. Furthermore, relaxation occurs spontaneously with an ultrashort time constant close to the vibrational period of strongly coupled phonons (molecular vibrations, in this case). It should thus be possible to time resolve the self-trapping time of a conjugated polymer with true one-dimensional confinement. The spontaneous geometrical relaxation is considered to be due to overdamped oscillations along the C–C and C=C bonds. Therefore, the formation time of the STE state in the overdamped model is expected to be 4–6 fs corresponding to a quarter of the typical oscillation period of the stretching modes. Hence, the time constant of 50 fs for MEH-PPV is much longer than expected. This can be explained by the effect of a large number of lower-frequency modes in the range 100–200 cm^{-1} and are consistent with the STE formation time.

3.2. Thermalization and electronic population relaxation

The spectra in Figure 1 have two peaks around 2.25–2.28 eV (545–555 nm) and 2.0 eV (620 nm). The latter forms a broad single peak for delay times of up to about 400 fs, but becomes a shoulder for longer delay times. The intensity of the higher-energy peak around 2.25–2.28 eV initially increases with delay and then begins to decrease. In these spectra, there are a large number of overlapping spectral lines in the regions around 1.72 and 2.25 eV. To investigate the presence of isosbestic points in these two spectral regions of 1.70 and 2.25 eV, which are expanded in Figure 3a and b, respectively. In the range 1.68–1.74 eV, there are 11 crossing points between two corresponding curves with adjacent delay times when the center delay time has a separation of 100 fs, while there are only four points in the range 2.21–2.27 eV of the same width. The high concentration of crossing points near 1.68 eV indicates that there is an isosbestic point in this range, but not in the other range. The absence of an isosbestic point implies that the spectral changes are not due to the population conversion between two spices with stable spectra but due to gradual shift.

The above smooth spectral shift is considered to be due to the thermalization process, which is expected to increases the average transition energy of bleaching spectrum. It is because as is seen from Figure 1, the laser is covering the high energy tail of the absorption spectrum. Then only the high energy vibronic levels are depleted and thermalization refills the depleted vibronic from the lower vibronic levels which are not substantially depleted. This increases the transition energy of the bleached spectral range. The relaxation to reach thermalized state can take place in the excited state also together with that in the ground state as discussed above. However the population reached by the laser only overlapping with the absorption tail is only in the lowest vibronic levels. Hence the extra energy in the excited state is small and the effect of relaxation among the vibronic levels in the excited state are expected to be much smaller than that in the ground state.

The population is considered to gradually approach the equilibrium Boltzmann distribution in this process. Thermalization is thought to occur in the following way. Intrachain thermalization among modes in the same chain occurs initially, while three-dimensional thermalization including vibrational energy transfer between neighboring chains occurs over a much long time scale (a few tens of picoseconds) with much lower frequencies. This energy shift is discussed in detail below.

As clearly shown in Figure 1, the spectral bandwidth of absorbance decreases with increasing probe delay time. As discussed above, the absence of an isosbestic point around 2.25 eV is considered to be responsible for the quasi-continuous spectral shift associated with the time-dependent change in the population distribution of the vibrational levels consisting of many modes. For longer delay times, thermalization is completed and relaxation to the ground state occurs. The peaks at about 1.97 and 2.25 eV may respectively correspond to the transitions $k'A_g \leftarrow 1^1B_u$ and $m'A_g \leftarrow 1^1B_u$ observed at 0.85 and 1.05 eV in PPV and at 0.9 and 1.5 eV in a soluble derivative of PPV (2,5-diocyloxy PPV; DOO-

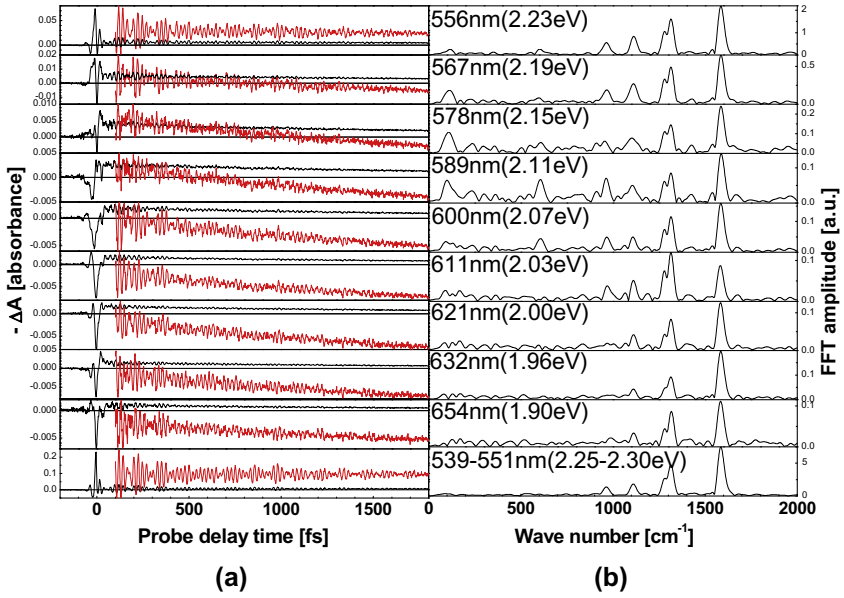

Figure 2. (a) Real-time traces of difference absorbance at ten typical wavelengths in the top nine columns and one at the bottom for the integrated spectral range of 539–551 nm (2.25–2.30 eV). In each of the real-time traces there are two curves, one of which is shown near the ordinate and the other is multiplied by 10. (b) The FT amplitude spectra of corresponding real-time traces.

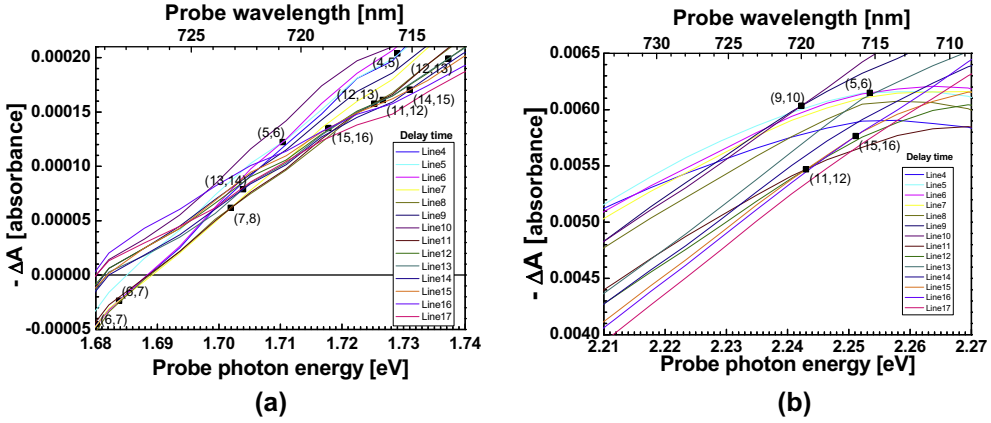

Figure 3. The time-resolved difference absorption spectra expanded in two spectral ranges of (a) 1.68–1.74 eV and (b) 2.21–2.27 eV.

PPV) investigated by the Vardeny group [41,42]. The transition energies of the two bands observed in the present study are much higher than those in the studies of [41,42] using a much lower probe photon energy than that the present case. Then the final states of the transitions, $k'A_g$ and $m'A_g$, may be located higher than the corresponding states of kA_g and mA_g; in other words, $k' > k$ and $m' > m$, where the level number of electronic states increases.

3.3. Mechanisms of observed coherent vibrations induced by ultrashort pulses

The Fourier transform of the time traces of the absorbance changes in the range of 556.2–654.0 nm (2.29–1.896 eV) is depicted in Figure 2b. It clearly exhibits the modulation of induced absorption due to coherent molecular vibrations. This is due to coupling of coherent molecular vibrations to the ground or excited states generated by the pump pulse through stimulated Raman or vibronic excitation. These interactions are sometimes referred to as Λ-type and V-type interactions, respectively [43]. There are three possible origins of the electronic transition intensity and/or the spectral change [44,34,45]. They can be classified into two categories: within and beyond the Condon approximation. The latter is the case when the transition probability depends on the coordinate(s) of the vibrational mode(s) and it is called the non-Condon case. The Condon case can be further classified into two categories: energy exchange and phase modulation by molecular vibrations.

These are explained in more detail below.

3.3.1. Energy exchange in the Condon approximation

Here, we perform a phenomenological analysis. For quantitative discussion, the probe photon energy dependence of the vibrational amplitude $\Delta A(\omega_{\text{probe}})$ can be described phenomenologically in terms of a stimulated Raman interaction in the ground state or a Raman-like interaction due to a wavepacket in the excited state by the following equations.[29,45]

$$\Delta A(\omega_{\text{probe}} = \omega_S) = C_{1S}|a(\omega_{\text{probe}}) - a(\omega_{\text{probe}} - \omega_v)| \quad (2)$$

$$\Delta A(\omega_{\text{probe}} = \omega_{AS}) = C_{1AS}|a(\omega_{\text{probe}}) - a(\omega_{\text{probe}} + \omega_v)| \quad (3)$$

$$A(\omega_{probe}) = L(\omega_{probe})(1 - 10^{\wedge}[-A(\omega_{probe})]) \quad (4)$$

Here C_{1S} and C_{1AS} are proportionality constants, ω_{probe} is the probe light frequency, and ω_v is the molecular vibration frequency. $L(\omega)$ is the laser spectrum and $a(\omega)$ is the absorbed laser spectrum, which is the frequency (ω) distribution of photons absorbed by the sample. $A(\omega)$ is the absorbance of the sample at ω. Eqs. (2) and (3) respectively correspond to the cases of pump/Stokes and pump/anti-Stokes interactions.

The above calculation is based on the assumption that the imaginary part of the third-order susceptibility $\chi_i^{(3)}$, which corresponds to the Raman interaction, can be expressed as

$$\chi_i^{(3)}(-\omega_2 : \omega_1, -\omega_1, \omega_2) = C_2(a(\omega_2) - a(\omega_1 = \omega_2 \pm \omega_v)), \quad (5)$$

where C_2 is a proportionality constant. The plus and minus signs in this equation correspond to the cases of pump/Stokes and pump/anti-Stokes interaction, respectively. The probe photon energy dependence can then be fitted using Eq. (5). Figure 4a shows the probe photon energy dependence of the Fourier vibrational amplitudes for six modes together with fitting curves obtained using the difference between the non-shifted and shifted absorbed photon energy distribution spectra given by Eq. (5). Since none of the fits are good, a Raman or Raman-like interaction mechanism cannot successfully explain the observations.

3.3.2. Phase modulation in the Condon approximation

The structure of a molecule changes during its vibrational period and the change in its electron distribution modulates the polarizability at the vibrational frequency. In particular, changes in the π electron distribution modulate the refractive index inducing molecular phase modulation (MPM) [46]. If this is the dominant mechanism, then the probe photon energy dependence should be proportional to the derivative of the time-resolved spectrum.

To study this mechanism, the vibrational amplitudes and the derivative of the induced absorption spectrum are shown in Figure 4b for comparison. The fitting curves are obtained from the first derivative of the time integrated spectrum from 135 to 185 fs (black curves) and from 1350 to 1800 fs (red curves). Therefore, phase modulation of the probe by molecular vibrations is not the dominant effect. It was also found that the sum of the two mechanisms cannot reproduce the probe wavelength dependence. Thus, it is considered that there is a complex combination of effects, including the above-mentioned mechanisms and the non-Condon effect.

3.3.3. Energy exchange between electronic states in the non-Condon approximation

The final mechanism is based on energy exchange between electronic states in the non-Condon condition [44]. It was clearly shown that the partially allowed Q-band is modulated by molecular-vibration mediated coupling with strongly allowed B-band. In the MEH-PPV system studied in this Letter has also strongly allowed ^1B_u state and ^1A_g state as clearly revealed by electro-absorption spectroscopy [47].

3.4. Dynamic mode coupling

Figure 5a shows the spectrogram obtained by integrating ΔA over the probe spectral range 1.91–1.98 eV using a Blackman window with a full width at half maximum of 360 fs. Previously dynamic mode coupling occurs though the existence of a frequency of amplitude modulation and/or frequency modulation common to several modes [28]. This mode coupling differs from the conventional static mode coupling. Dynamic mode coupling is induced by short pulse excitation of vibrational modes, which inevitably generates dynamically varying distributions of vibration modes [28].

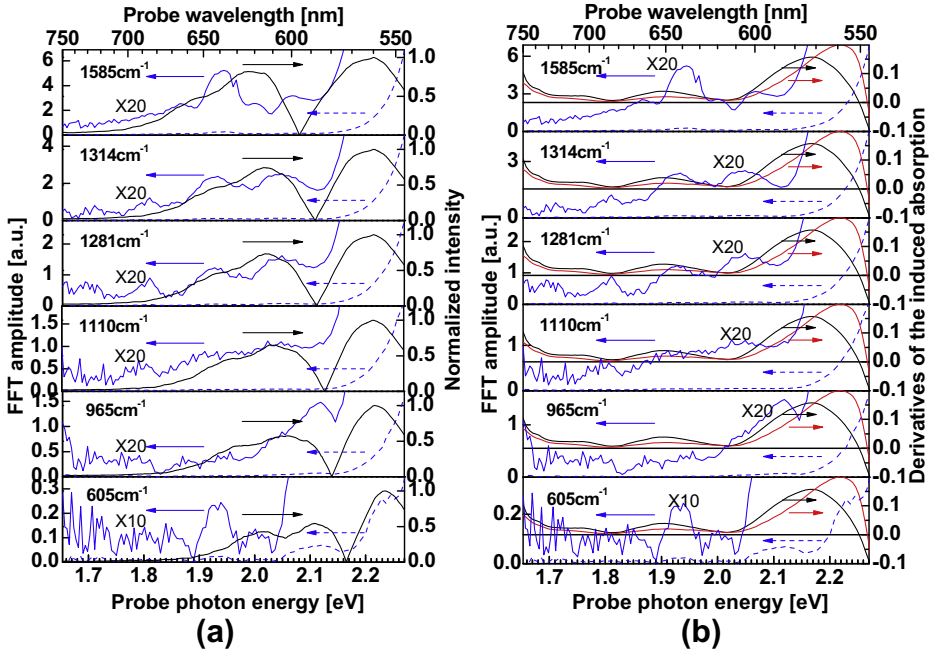

Figure 4. (a) The probe photon energy dependence of Fourier vibrational amplitudes (blue dashed curves and 20-times multiplied amplitudes (blue solid curves) together with fitting curves (black curves) obtained using the difference between the non-shifted and shifted absorbed photon energy distribution spectra given by Eq. (2). (b) Vibrational amplitudes (blue dashed curves and 20-times multiplied amplitudes (blue solid curves) and the fitting curves obtained using the derivative of time-integrated induced absorption spectrum from 135 to 185 fs (black curves) and those using the data from 1350 to 1800 fs (red curves). (For interpretation of the references to color in this figure legend, the reader is referred to the web version of this article.)

This modulates the frequency and amplitude of the excited vibrational modes.

The first moment of the frequency of the Fourier-power spectrum of the mode was calculated over the distribution function of each Fourier-power spectrum. The mean frequency at each gate-delay time was calculated from the first moment (Figure 5a). The Fourier amplitude spectrum of the mean frequency corresponding to frequency of the vibrational frequency modulation (FM) around 1584 cm^{-1} is shown in Figure 5c. In addition, the gate-delay time dependence of the peak amplitude of the Fourier spectrum corresponding to amplitude modulation (AM) is also plotted in Figure 5b and its Fourier amplitude spectrum is shown in Figure 5d. The FM and AM frequencies were found to be 60–70, 113, 170 cm^{-1} and 66, 112, 172 cm^{-1}, respectively. The components of the two pairs of three frequencies are all close to each other and are considered to be from same origins. These low-frequency modes are thought to represent various bending modes and to contribute to the stretching modes through frequency and amplitude modulation. This implies that the three low-frequency modes are dynamically coupled to the stretching mode that has a frequency of 1584 cm^{-1}. Since we are exciting a linear combination of eigenmodes rather than a single eigenmode, the excited modes are all coupled to each other so that their amplitudes and instantaneous frequencies vary with time. The mode distribution is determined by the ultrashort pulse laser spectrum and the Franck–Condon factor. Therefore, after impulsive excitation, energy exchange occurs through dynamic mode coupling [28].

3.5. Vibrational energy and phase relaxation

To study the vibrational energy relaxation associated with thermalization (see Section 3.2), the first moment of the induced absorption was calculated using the $\Delta A(\omega)$ spectrum in the range of 1.8–2.2 eV as shown in Figure 6a. The moment can be reproduced by as follows:

$$\Delta E(t_D) = (\Delta E(0) - \Delta E(\infty))\exp(-t_D/\tau_e) + \Delta E(\infty), \quad (6)$$

where τ_e is the relaxation time, $\Delta E_{extr} = |\Delta E(0) - \Delta E(\infty)|$ is the initial extra energy to be relaxed, and $\Delta E(\infty)$ is the final energy after thermalization.

From the best fit to the observed curve using Eq. (6), the values are determined to be $\tau_e/\Delta E_{extr}$ ~500 fs/7 meV = 8.9 fs/cm^{-1}, ΔE_{extr} = 7 meV, and $\Delta E(\infty)$ = 2.08 eV. The value of $\tau_e/\Delta E_{extr}$ implies that the time required for relaxation from the non-equilibrium state to the thermally relaxed state by an energy of 7 meV is about 500 fs.

To calculate the contribution of each coupled mode to energy relaxation, the fitted curve was subtracted from the observed curve of the first moment and a Fourier transform was performed. Assuming that the Fourier power is proportional to the contribution to energy relaxation, the fractional contribution of each mode was calculated (see Figure 6b and Table 1a). Using the determined parameters and fractional contributions, the relaxation time required for each mode (i.e., the contribution of each mode to the energy relaxation) was calculated. Based on these results, the number of vibrations required for each mode to reach the thermalization energy of $(1-1/e)\Delta E_0$ was calculated

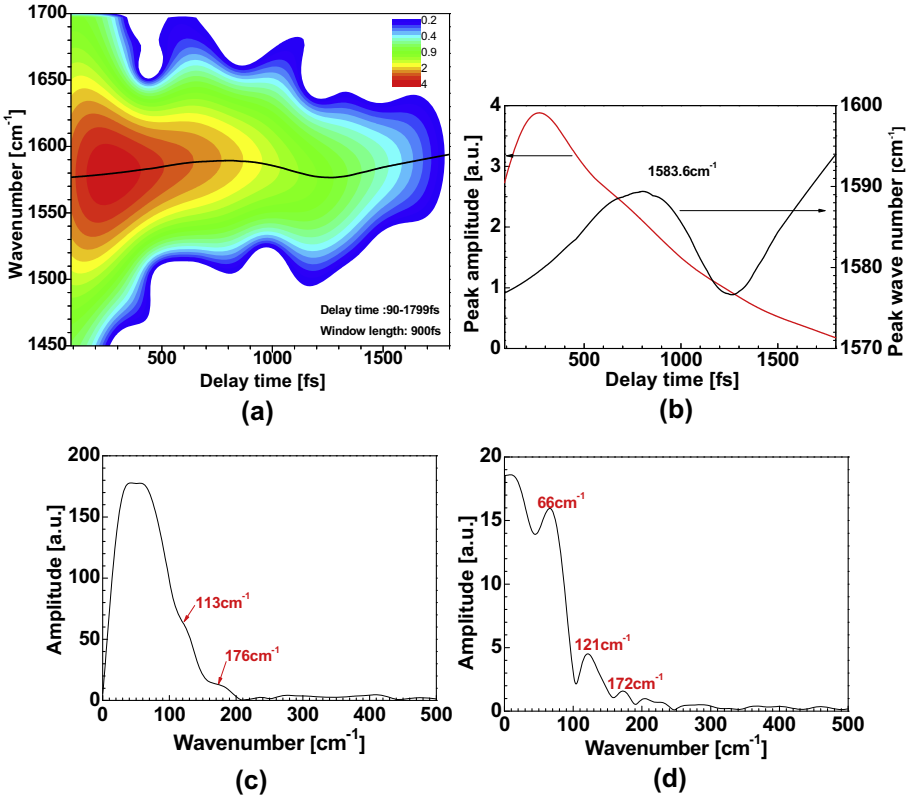

Figure 5. (a) The spectrogram of frequency component around 1580 cm^{-1} calculated the integrated difference absorbance ΔA over 1.91–1.98 eV range with the 900 fs Blackman window corresponding to 360 fs FWHM and sliding peak from 90 to 1799 fs. The curve is the spectral peak wavenumber tracked along the gate delay time. (b) Instantaneous wave number (black curve) and time-dependent amplitude (red curve) determined by intensity-peak tracking of the spectrogram shown in Figure 6. (c) The Fourier amplitude spectra of the instantaneous wave number corresponding to the frequency modulation (FM) of the peak around 1580 cm^{-1}. (d) Fourier amplitude spectra of peak amplitude modulation (AM) of the peak shown in the spectrogram depicted in (a) after the time-dependent amplitude curve being subtracted with a single exponential function. (For interpretation of the references to color in this figure legend, the reader is referred to the web version of this article.)

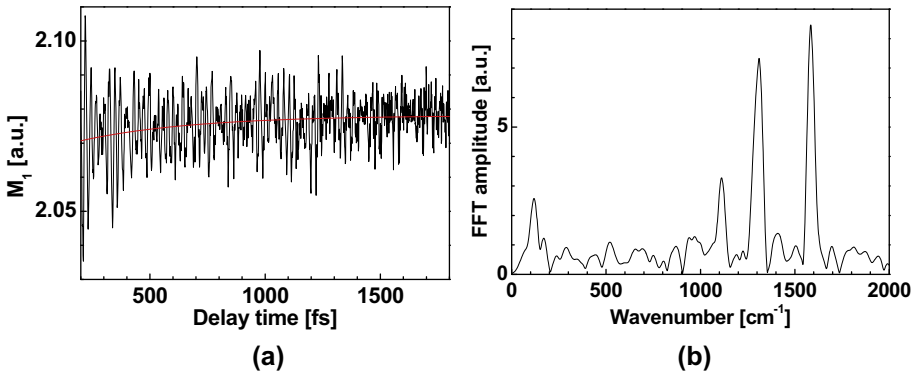

Figure 6. (a) The probe delay time dependence of the first moment M_1 calculated using the $\Delta A(\omega)$ spectrum in the range of 1.8–2.2 eV. (b) The FT amplitude of the time-dependent first moment shown in (a).

Table 1a
The Raman shift wave numbers of several intense modes and the real-time vibrational wave numbers of Fourier transform of the integrated real time traces in three different ranges of 1.65–1.67 eV ($\Delta A < 0$) and 1.8–2.2 eV and 1.91–1.98 eV ($\Delta A > 0$). The listed data of Raman[(1)] are measured in the present study using an Ar laser at 488 nm as a pump. The data and assignments shown in the column of "Raman[(2)]" are from Bruevich et al. J. Chem. Phys. 127 (2007) 104905, Yang et al. Rev. Adv. Mater. Sci. 15 (2007) 144, That et al. J. Lumin. 128 (2008) 2031.

Peak wave number [cm^{-1}]					Vibration mode[(2)]
Raman[(1)]	Raman[(2)]	$\Delta A < 0$	$\Delta A < 0$		
		1.65–1.67 eV	1.8–2.2 eV	1.91–1.98 eV	
	~600		607	614	
921			911		
971	966, 969	980	958	969	Out-of-plane CH bending mode of the vinylene group.
1115	1112, 1115			1112	Mixtures of C–C stretching and C–H in plane bending.
1285	1282, 1283	1282	1278		C=C stretching band of benzene ring.
1314	1310		1308	1311	
	1547, 1557				
1588	1582,	1581	1593	1585	C–C stretching band of benzene ring.
1627	1623, 1624, 1625	1629		1624	C=C stretching band of the vinyl group.

Table 1b
The fractional contribution of each vibrational mode to energy relaxation.

Frequency [cm^{-1}]	Number of vibrations if the mode is the only channel to energy relaxation	Fractional contribution	Number of vibrations due to each mode for the energy relaxation ($\times 10^2$)
965	14.5	0.03	48
1110	16.5	0.05	31
1280	19.2	0.07	27
1315	19.7	0.16	12
1585	23.8	0.35	7

(Table 1b). Table 1b shows that the population relaxation time (~500 fs) for the vibrational level of each mode is about 20 times longer than the phase relaxation time (25 fs). This means that even after the vibrational coherence decays, the population of that level is maintained.

3.6. Electronic phase relaxation time

According to the theory describing the nonlinear response of absorbance due to photoexcitation in pump–probe experiments, there are three typical time ranges [48]. Here, we applied this method to determine the dephasing time of the coherence between the exciton and ground states. The relaxation times in Figure 7 have a strong dependence on the probe photon energy. The short lifetimes in the spectral ranges other than ~1.95 eV are due to contamination by coherent artifacts, which have the correlation width

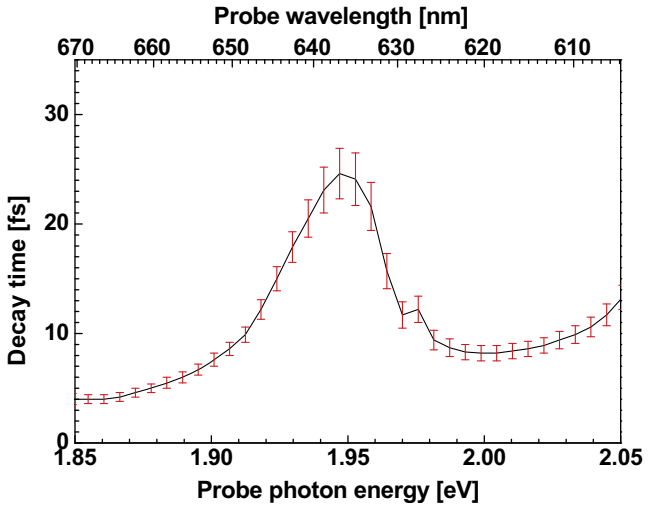

Figure 7. Decay time spectrum determined for the negative-delay time data at 34 different probe photon energies in the range from 1.85 to 2.05 eV. The error bars show the standard deviations in the fitting calculation to a single exponential function.

of the pump and probe pulses. Therefore, as in our previous study, we took the longest one 25 ± 2 fs as the actual electronic dephasing time.

4. Conclusion

We utilized sub-6-fs laser pulses to investigate relaxation of exciton in MEH-PPV and the vibrational levels of various modes coupled to the transitions between the ground and excited states. The mechanism for coupling between the electronic states and coherent vibrations was found to be a non-Condon type from the probe photon energy dependence of the vibrational amplitude determined from the Fourier amplitude spectrum. Ultrafast geometrical relaxation due to self-trapping was for the first time determined to be 50 ± 23 fs in MEH-PPV. Ultrafast electronic dephasing time is determined as 25 ± 2 fs. Spectrographic analysis revealed dynamic coupling among the high-frequency and low-frequency modes. The vibrational population relaxation dynamics was determined from the mean transition energy of the excited state absorption. The population relaxation time associated with descent of the five most strongly coupled vibrational levels in the energy ladder, corresponding to a relaxation of 7 meV, was determined as 500 fs. Subsequently, the contribution to vibronic energy relaxation was estimated for the five modes. The energy ladder descent time of about 500 fs is 20 times longer than the phase relaxation time of 25 fs. This means that even after the phase of vibrational coherence of any given level decays (due to homogeneous or inhomogeneous broadening), the population of that level is maintained.

Acknowledgments

This Letter was supported by the NSC, Taiwan (NSC 98-2112-M-009-001-MY3), and the Ministry of Education (MOE ATU). A part of this Letter was supported the Institute of Laser Engineering, Osaka University (No. A3-05).

References

[1] G.A.M. Sáfar, F.A.C. Oliveira, L.A. Cury, A. Righi, P.L.M. Barbosa, P. Dieudonné, F.S. Lameiras, J. Appl. Polym. Sci. 102 (2006) 5620.
[2] R.H. Friend et al., Nature 397 (1999) 121.
[3] F. Hide, M.A. Díaz-García, B.J. Schwartz, A.J. Heeger, J. Acc. Chem. Res. 30 (1997) 4301.
[4] L.J. Rothberg, A.J. Lovinger, J. Mater. Res. 11 (1996) 3174.
[5] T. Kobayashi (Ed.), Nonlinear optics of organics and semiconductors, Springer proceeding physics, vol. 36, Springer, Berlin, 1989.
[6] S. Etemad, Z.G. Soos, in: R.J.H. Clark, R.E. Hester (Eds.), Spectroscopy of advanced materials, Wiley, New York, 1991, p. 87.
[7] R.F. Mahrt, T. Pauck, U. Lemmer, U. Sieger, M. Hopmeier, R. Hennig, H. Bässler, E.O. Göbel, Phys. Rev. B 54 (1996) 1759.
[8] A.J. Heeger, S. Kivelson, J.R. Schrieffer, Rev. Mod. Phys. 60 (1988) 781.
[9] P.L. Burn, A.B. Holmes, A. Kraft, D.D.C. Bradley, A.R. Brown, R.H. Friend, R.W. Gymer, Nature 356 (1992) 47.
[10] G.R. Hayes, I.D.W. Samuel, R.T. Phillips, Phys. Rev. B 52 (1995) R11569.
[11] B. Park et al., Adv. Mater. 19 (2007) 4353.
[12] M.E. Gershenson, V. Podzorov, A.F. Morpurgo, Rev. Mod. Phys. 78 (2006) 973.
[13] T. Blythe, D. Bloor, Electrical properties of polymers, Cambridge University Press, Cambridge, 2002.
[14] C. Brabec, V. Dyakonov, J. Parisi, N.S. Sariciftci (Eds.), Organic photovoltaics: concepts and realization, Springer, Berlin, 2003.
[15] N. Tessler, G.J. Denton, R.H. Friend, Nature 382 (1996) 695.
[16] G. Hadziioannou, P.F.V. Hutten (Eds.), Semiconducting polymers, Wiley-VCH, Weinheim, 2007.
[17] A. Köhler et al., Nature 392 (1998) 903.
[18] B.J. Schwartz, Annu. Rev. Phys. Chem. 54 (2003) 141.
[19] M. Liess, S. Jeglinski, Z.V. Vardeny, M. Ozaki, K. Yoshino, Y. Ding, T. Barton, Phys. Rev. B 56 (1997) 15712.
[20] S. Abe, J. Phys. Soc. Jpn. 58 (1989) 62.
[21] R. Chang, M. Hayashi, S.H. Lin, J.-H. Hsu, W.S. Fann, J. Chem. Phys. 115 (2001) 4339.
[22] W. Barford, I. Boczarow, T. Wharram, J. Phys. Chem. A 115 (2011) 9111.
[23] T. Cassano et al., Opt. Mater. 21 (2003) 325.
[24] F.C. De Schryver, S. De Feyter, G. Schweitzer (Eds.), Femtochemistry, Wiley-VCH, Weinheim, Germany, 2001.
[25] A. Douhal, J. Santamaria (Eds.), Femtochemistry and femtobiology, World Scientific, Singapore, 2001.
[26] A.W. Castleman, M.L. Kimble (Eds.), Femtochemistry VII fundamental ultrafast processes in chemistry, physics, and biology, Elsevier, The Netherlands, 2006.
[27] T. Kobayashi, T. Saito, H. Ohtani, Nature (London) 414 (2001) 531.
[28] T. Kobayashi, A. Shirakawa, H. Matsuzawa, H. Nakanishi, Chem. Phys. Lett. 321 (2000) 385.
[29] N. Ishii, E. Tokunaga, S. Adachi, T. Kimura, H. Matsuda, T. Kobayashi, Phys. Rev. A 70 (2004) 023811.
[30] X. Yang, T.E. Dykstra, G.D. Scholes, Phys. Rev. B 71 (2005) 045203.
[31] A. Ruseckas, I.D.W. Samuel, Phys. Status Solidi C 3 (2006) 263.
[32] A. Ruseckas, P. Wood, I.D.W. Samuel, G.R. Webster, W.J. Mitchell, P.L. Burn, V. Sundström, Phys. Rev. B 72 (2005) 115214.
[33] J. Zhang, Z. Wang, T. Kobayashi, Phys. Rev. B 77 (2008) 153202.
[34] T. Kobayashi, J. Zhang, Z. Wang, New J. Phys. 11 (2009) 013048.
[35] T. Kobayashi, M. Yoshizawa, U. Stamm, M. Taiji, M. Hasegawa, J. Opt. Soc. Am. B 7 (1990) 1558.
[36] A. Shirakawa, I. Sakane, M. Takasaka, T. Kobayashi, Appl. Phys. Lett. 74 (1999) 2268.
[37] A. Baltuska, T. Fuji, T. Kobayashi, Opt. Lett. 27 (2002) 306.
[38] X. Yang, T.E. Dykstra, D. Scholes, Phys. Rev. B 71 (2005) 045203.
[39] H. Matsuzawa, S. Okada, H. Matsuda, H. Nakanishi, Chem. Lett. 26 (1997) 1105.
[40] H. Tanaka, M. Inoue, E. Hanamura, Solid State Commun. 63 (1987) 103.
[41] R. Österbacka, M. Wohlgenannt, M. Shkunov, D. Chinn, Z.V. Vardeny, J. Chem. Phys. 118 (2003) 8905.
[42] S.V. Frolov, M. Liess, P.A. Lane, W. Gellermann, Z.V. Vardeny, M. Ozaki, K. Yoshino, Phys. Rev. Lett 78 (1997) 4285.
[43] J. Du, T. Teramoto, K. Nakata, E. Tokunaga, T. Kobayashi, Biophys. J. 101 (2011) 995.
[44] H. Kano, T. Saito, T. Kobayashi, J. Phys. Chem. A 106 (2002) 3445.
[45] T. Kobayashi, Z. Wang, IEEE J. Quant. Electron. 44 (2008) 1232.
[46] N. Zhavoronkov, G. Korn, Phys. Rev. Lett. 88 (2002) 203901.
[47] S.J. Martin, D.D.C. Bradley, P.A. Lane, H. Mellor, Phys. Rev. B 59 (1999) 15133.
[48] T. Kobayashi, J. Du, W. Feng, K. Yoshino, Phys. Rev. Lett. 101 (2008) 037402.